IEEE Access
Multidisciplinary | Rapid Review | Open Access Journal

Received April 10, 2018, accepted May 3, 2018, date of publication May 9, 2018, date of current version June 5, 2018.

Digital Object Identifier 10.1109/ACCESS.2018.2834726

Novel Microwave Sensors Based on Split Ring Resonators for Measuring Permittivity

KUIWEN XU[1,2], (Member, IEEE), YANG LIU[1], SHICHANG CHEN[1], (Member, IEEE), PENG ZHAO[1], (Member, IEEE), LIANG PENG[1], LINXI DONG[1,3,4], AND GAOFENG WANG[1], (Senior Member, IEEE)

[1]Key Laboratory of RF Circuits and Systems, Ministry of Education, Microelectronics CAD Center, College of Electronics and Information, Hangzhou Dianzi University, Hangzhou 310018, China
[2]State Key Laboratory of Millimeter Waves, Southeast University, Nanjing 210096, China
[3]State Key Laboratory of Functional Materials for Informatics, Shanghai Institute of Microsystems and Information Technology, Chinese Academy of Sciences, Shanghai 200050, China
[4]State Key Laboratory for Manufacturing Systems Engineering, Xi'an Jiaotong University, Xi'an 710049, China

Corresponding author: Gaofeng Wang (gaofeng@hdu.edu.cn)

This work was supported in part by the National Natural Science Foundation of China under Grant 61601161, Grant 61331007, Grant 61601163, Grant 61601160, and Grant 61411136003 and in part by the Key Research and Development Plan Project of Zhejiang Province under Grant 2018C01036.

ABSTRACT Measuring the electromagnetic properties of materials has important applications in many fields. In this paper, two electrically small sensors based on the split ring resonators (SRRs) with extended long legs, i.e., two-layer and three-layer magnetic coupled SRRs, are proposed to measure the permittivity of small samples of unknown materials. By virtue of the characteristics of SRRs, the proposed resonators have several merits, such as extremely compact size ($0.067\lambda_0 \times 0.067\lambda_0$ and $0.052\lambda_0 \times 0.052\lambda_0$ for two-layer and three-layer magnetic coupled SRRs, respectively), high quality factor (Q), and stable resonance. Especially, the proposed three-layer magnetic coupled sensor with opposite splits on the SRRs is able to further improve the quality factor and have better stability compared with the two-layer coupled sensor. By different shifting resonant frequencies instead of the single ones and the polynomial fitting method, the proposed sensors can accurately calculate the unknown permittivity. Simulated and experimental results have validated the efficacy of the proposed approach and designs. With the features of compact size and lower far-field radiation, the proposed resonators can be combined with various permittivity measurement algorithms to improve the measurement accuracy in a wide range of environments beyond the specific experimental setup.

INDEX TERMS Permittivity measurement, resonators, split ring resonators (SRRs), magnetic coupling, far-field radiation suppression.

I. INTRODUCTION

Permittivity is an important parameter to describe the electromagnetic properties of the dielectric materials. With rapid development of microwave circuit technology, precise measurement of the complex permittivity of a material plays a significant role for microwave applications, which has attracted more and more attentions from both academia and industry [1], [2]. Recently, a variety of techniques for measuring dielectric constant have been proposed for different frequency bands in the literature [3]–[21]. In the radio frequency and microwave bands, the methods for measuring permittivity can generally be classified into two categories, i.e., the non-resonance methods and the resonance methods. The non-resonance methods mainly include the RF-circuit method [3]–[5], the transmission and reflection method [6], [7], the open-ended coaxial probe method and the free space method [8]–[10].

Owing to merits such as low cost, easy integration, real-time monitoring, and easy miniaturization, the resonance methods have drawn great interests [11]–[16]. The resonance methods primarily include two types: the resonant perturbation methods [11], [12] and the resonator methods [13]–[16]. In the resonant perturbation methods, a dielectric sample is placed in a resonant cavity, which affects its resonance frequency and quality factor (Q). The permittivity of the dielectric sample can be then obtained by measuring the resonant frequency shift and the Q variation of the cavity. However, it needs a special waveguide cavity, in which the sample

under test (SUT) can be placed conveniently. In the resonator methods, for both contact and non-contact measurements, the SUT can be considered as a part of the resonator and the permittivity can be deduced from the relative resonant frequency shift, which has a relatively high accuracy and sensitivity [17]–[21].

In order to obtain high precision in measurement, the resonators with high Q are preferred [12], [15], [22]. So far, various designs of the resonators have been proposed. In [12], only one single split ring resonator (SRR) was used between the transmitting and receiving probes to extract the permittivity of dielectric samples. However, it is difficult to keep the probes fixed during measurements and the dielectric sample must have at least one flat surface greater than or equal to the area of the SRR structure. In [13] and [14], the microwave sensors based on complementary split-ring resonators (CSRRs) etched on the ground plane of a microstrip line were proposed for dielectric characterization of planar materials. The dual port design needs relatively large electrical size, which is particularly suitable for the layered dielectric structure. In [15], planar microwave sensors were introduced by virtue of symmetrical split ring resonator (SSRR) with high sensitivity and very high Q. The electric coupling with microstrip line was used for excitation, which suffers far-filed radiation, and the measured transmission coefficient was thus susceptible to interference. In [16], a patch antenna was used as the sensor for detection of the layer thickness and the permittivity. Although this sensor may have a good resolution for the thickness and dielectric constant of multilayer dielectrics under an ideally isolated experimental environment, some unavoidable errors due to its very high far-field radiation can be caused by the surrounding environment.

The SRR is a classic kind of electrically small resonator that can be composed of the metamaterial with negative permeability and negative permittivity [23], and widely applied in RF microwave devices. The electromagnetic properties of SRRs make them very easy to be coupled by the electric field or the magnetic field in the near field range. In addition, the electrically small and high-Q-factor characteristics of SRRs make them capable of effectively suppressing the far-field radiation. Therefore, many designs for the permittivity measurement with electrically coupled SRRs have been springing up [4], [22], [24].

Different from those in the previous literature, novel resonators based on magnetic coupled SRRs are proposed herein in this work. In virtue of excitation with electrically small loop, which can be considered as a magnetic dipole, two kinds of magnetic coupled resonators, i.e., two- and three-layer resonators, based on SRRs are presented. The two-layer magnetic coupled resonator with electrical size of $0.067\lambda_0 \times 0.067\lambda_0$ (λ_0 is the wavelength of the resonant frequency) and high Q value of about 250 is firstly analyzed. In order to further improve the stability and suppress the far-filed radiation of the opening resonators, a three-layer resonator with an additional anti-symmetric SRR placed on its bottom is constructed. Compared with the two-layer resonator, the three-layer resonator has smaller electrical size ($0.052\lambda_0 \times 0.052\lambda_0$), higher Q value (about 345), and better stability and robustness against to the noise. With those merits above and the opening configuration but strong ability in anti-interference, the proposed resonators are no longer experimental devices but practical ones that can be used in a wide range of industry applications.

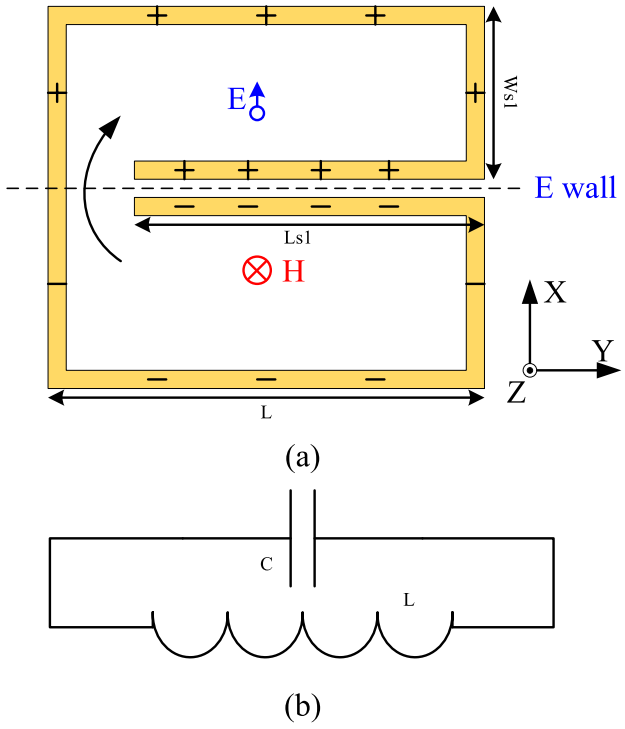

FIGURE 1. (a) SRR unit-cell: basic cell size, orientation of polarized field, distribution of charge and current, and boundary conditions at the plane of symmetry, (b) *LC* equivalent circuit model.

The rest of this paper is organized as follows. In Section II, the basic theory and underlying mechanism of magnetic coupled SRRs are explained. Then, the design principle of the two resonators is presented and their performances are analyzed in Sections III and IV. In Section V, the simulated and measured results of the two resonators are compared and the retrieval method of dielectric constant is discussed. Finally, the conclusions are drawn in Section VI.

II. THEORY

The metamaterial element consists of a square open ring and two extended parallel long stubs, which is considered as a novel split ring with extended long legs, as depicted in Fig. 1(a). As shown in Fig. 1(a), when the novel split ring is excited by an external time-varying magnetic field directed in the axial direction (i.e., Z-axis), an electromotive force around the ring is generated, which produces a current in the ring. By virtue of the long extended parallel metal stubs, the current flows through the slot between the stubs in the form of displacement current. The displacement current is

concentrated along the long slot while the electric filed is the maximum between the stubs. Actually, the symmetrical plane (i.e., YZ plane) of the split ring can be considered as a virtual electrical wall. As is well known, the classic SRRs show simultaneously magnetoelectric response, where electric dipole and magnetic dipole are along the Y-axis and the Z-axis in Fig. 1, respectively [25]. The magnetic dipole is the dominant excitation at the resonance. However, owing to the pair of extended long stubs, the novel SRR acts as an electric dipole, which is dominant at the resonance. As the classic SRRs, owing to the electrically small size, the quasi-static analysis method can be applied. The performance of the novel SRR can be modeled as a self-resonant closed LC circuit as shown in Fig. 1(b).

In the Fig. 1(b), inductance L represents the self-inductance of SRR, and capacitance C represents the distributed capacitance between the pair of the parallel metal stubs that can be expressed as

$$C = LsC', \tag{1}$$

where C' is the per-unit-length capacitance along the parallel metal strip and Ls is the length of the parallel stubs. The resonant frequency f of SRR can be calculated as

$$f = \frac{1}{2\pi\sqrt{LC}}. \tag{2}$$

In order to excite the novel split ring, a closed ring is usually used for inducing the magnetic fields along the Z-axis as mentioned in [26]. Different from the antenna in [26], however, a resonator with a high Q and a low radiation efficiency is herein preferred.

For the electrically small radiator with multi-layer coupling SRRs, the total electric power P_{total} provided by the coupled loop source can be expressed as

$$P_{total} = P_{res} + P_s + P_{rad}, \tag{3}$$

where P_{res} is the Ohmic loss of the conductor, P_s is the dielectric loss, and P_{rad} is the far-field radiated power. Then the radiation efficiency can be expressed as

$$\eta = \left(1 + \frac{P_{res}}{P_{rad}} + \frac{P_s}{P_{rad}}\right)^{-1}. \tag{4}$$

According to the analysis in [26], the radiation efficiency can be calculated as follows:

$$\eta = \left((1 + \frac{12\pi R}{k^4 S^2}\sqrt{\frac{\varepsilon_0}{\mu_0}}\frac{\sum |I_n|^2}{\left(\sum I_n\right)^2} + \frac{12\pi}{k^4 S^2}\sqrt{\frac{\varepsilon_0}{\mu_0}}\frac{P_s}{\left(\sum I_n\right)^2})\right)^{-1}, \tag{5}$$

where S is the closed surface of an arbitrary volume containing the resonator, R is the resistance of each SRR, and I_n is the current of the n-th SRR. Therefore, if the current in the multilayer SRRs is in the same direction, the radiation efficiency will increase, otherwise the efficiency will decrease.

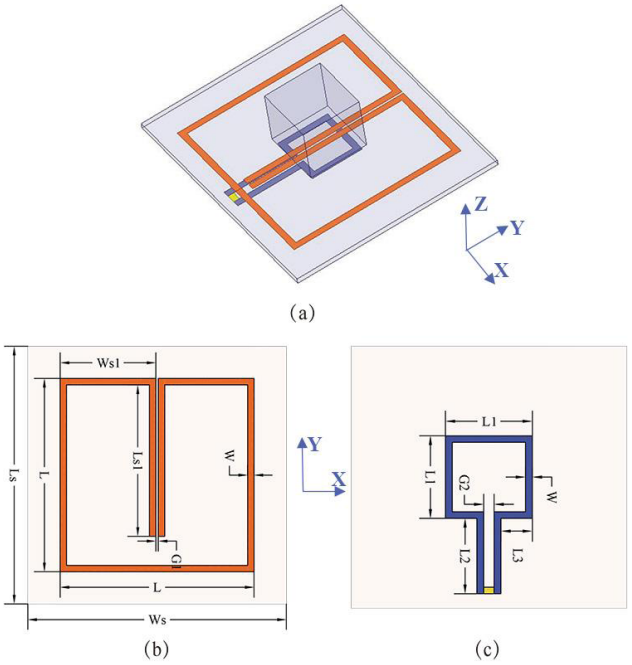

FIGURE 2. Configuration of the two-layer magnetic coupled SRRs resonator. (a) Three-dimensional view, (b) top layer view, (c) bottom layer view.

TABLE 1. Detail parameters of the two-layer resonator.

Parameters	Ls	Ws	L	Ls1	Ws1	W
Unit(mm)	40	40	30	23.5	14.815	1
Parameters	L1	L2	L3	G1	G2	
Unit(mm)	12.6	10.5	5.55	0.37	1.5	

III. DESIGN OF RESONATORS

In order to achieve accurate measurement of the dielectric constant via electromagnetic wave, the resonator with high sensitivity and high Q characteristics is required. Meanwhile, to keep the size of the resonator as compact as possible, the electrically small resonator is preferred owing to its sub-wavelength size and much higher Q value. As is well known, the metamaterial is a good candidate for the sub-wavelength resonator. Herein, the novel SRRs with deep sub-wavelength dimensions are utilized to construct the resonator.

Based on those, the two-layer magnetic coupled resonator is shown in Fig. 2, which consists of three parts, i.e., the 1.0 mm thick F4BM220 substrate ($\varepsilon_r = 2.2$, $\mu_r = 1$, loss tangent = 0.003), the novel SRRs at the top layer and the coupled loop on the bottom layer. The electrical size of the resonator is about $0.067\lambda_0 \times 0.067\lambda_0$ (λ_0 is the wavelength of the resonant frequency), where the detailed dimensions are given in Table 1. With excitation through the magnetic closed loop, it is perfect to make it work in electrically small mode.

The three-dimensional (3-D) configuration of the proposed resonator is shown in Fig. 2(a). The sample under test (SUT) with the dimension $10 \times 10 \times 10$ mm^3 is placed on the resonator. The simulated reflection coefficients (i.e., S_{11}) of

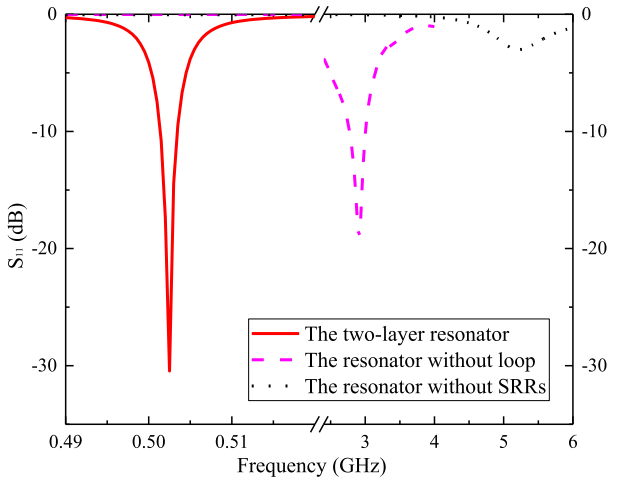

FIGURE 3. Simulated reflection coefficients of three kinds of resonators.

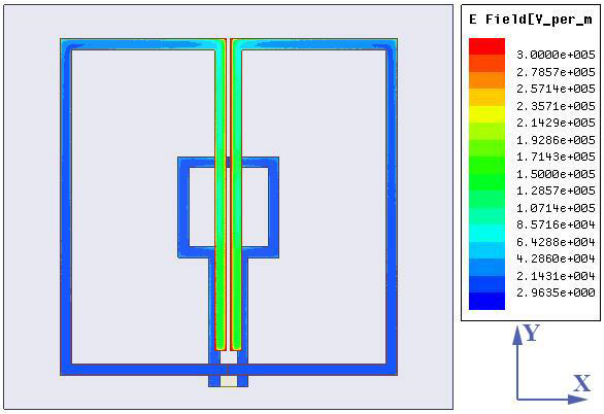

FIGURE 4. Electric field distributions of the two-layer resonator at 0.5024 GHz.

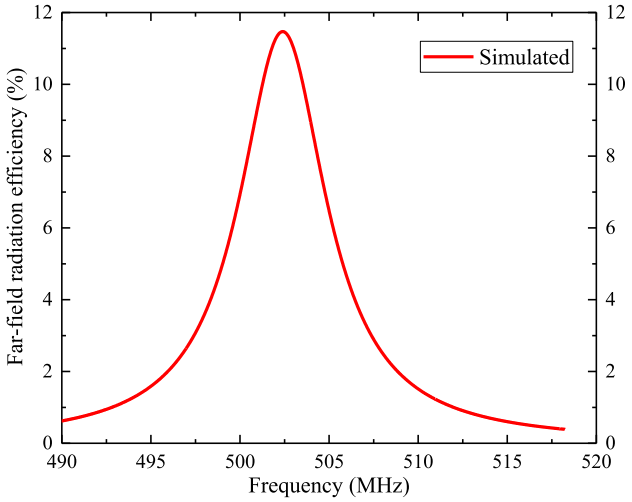

FIGURE 5. Far-field radiation efficiency of the two-layer resonator.

three kinds of resonators (i.e., the proposed two-layer resonator, the resonator without loop, and the resonator without SRRs) are plotted in Fig. 3. The proposed two-layer resonator operates with a −10 dB impedance bandwidth from 0.5014 GHz to 0.5034 GHz, i.e., 2 MHz (about a 0.4% fractional bandwidth and equivalent to a Q-factor of 250).

To study the interactions of the coupled loop and the novel SRRs, the resonator without coupled loop and the resonator without SRRs are also investigated, as shown in Fig. 3. As mentioned in [27], the split ring and the closed loop operate at the odd mode and the even mode respectively. Without SRRs, the loop operates at the resonant frequency: 5.217 GHz, with a poor impedance matching ($|S_{11}| \geq -3.0211$ dB). For the resonator without loop, the SRRs resonance at 2.911 GHz, with better impedance matching ($|S_{11}| \geq -19.1796$ dB). When both the coupling loop and the SRRs present, an extra lower resonant frequency, i.e., 0.5024 GHz, can be generated, which is 90.37% offset relative to the resonant frequency of the loop. With the sub-wavelength resonator, an excellent impedance matching ($|S_{11}| \geq -41.0895$ dB) and 0.4% fractional bandwidth (extra 250 Q value) can be finally achieved.

The SUT is assumed to be placed at the center of the upper layer of the resonator, where the electric field distribution is the maximum on the top of the SRR at 0.5024 GHz as illustrated in Fig. 4. However, the electric field at the coupled loop on the bottom looks much weaker and is evenly uniform throughout the sub-wavelength loop. When the electric field in the electrically small loop with the size of sub-wavelength remains uniform, such a loop can be equivalent to a magnetic dipole. Therefore, it is further illustrated that the proposed two-layer magnetic coupled SRRs resonator works at electrically small mode. With strong near-filed coupled interaction between the loop on the bottom and the SRR on the top, the electrically small SRR is excited by the magnetic fields along the Z-axis. As the analysis in the Section II, the two stubs are close to each other and long enough, the electric field is concentrated along the pair of extended stubs so as to attain the maximum owing to the displacement current. Therefore, it is reasonable to infer that placing the SUT in the maximum electric field (along the pair of stubs) results in higher sensitivity to the SUT.

However, owing to the characteristics of the resonator with open environment, the far-field radiation efficiency of the resonator is an important parameter of concerning. Since the SUT is usually placed as close as possible to the resonator, to a large extent, the sensitivity comes from the perturbation of the near field. If far-field radiation is strong, a small disturbance from the environment can interfere with the measurement. In order to avoid the far-field impact on the measurement, it is necessary to suppress the far-filed radiation as much as possible. When the impedance matching is good, the far-filed radiation efficiency can be a good indicator on the degree of the suppression of far-field radiation. From Fig. 5, one can see that the maximum radiation efficiency can attain as high as 12%. Such low radiation efficiency implies a low level of far-field power radiation, which can in turn

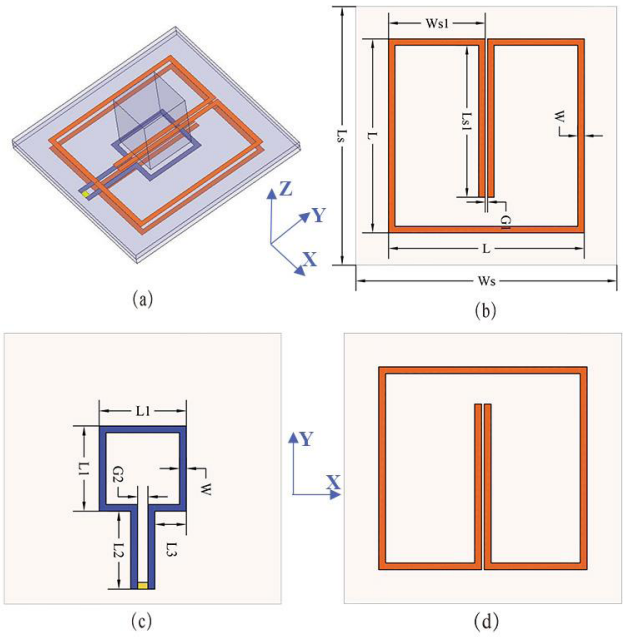

FIGURE 6. Configuration of the three-layer magnetic coupled SRRs resonator. (a) 3-D view, (b) top layer view, (c) mid-layer view, (d) bottom layer view. (The size of the bottom layer is the same as the top layer, and all the dimensions are the same as the Table 1).

reduce the reflection or scattering of nearby objects from the environment. As a result, the measurement system has very good noise immunity. Although the radiation efficiency is quite low, it is shown later that the disturbance of the environment can be further reduced by the improved three-layer magnetic coupled resonator, which is discussed in the following Section.

IV. THREE-LAYER RESONATOR DESIGN

While the above two-layer magnetic coupled SRRs resonator achieves the expected goals of high Q factor, high sensitivity and low far-field radiating level, it would be more desirable to have an even smaller electrically size, better performance and higher stability for the measurement. Consequently, a three-layer magnetic coupled resonator based on SRRs is proposed by virtue of the methodology of the coupled resonator introduced in Sections II. This design prototype, as shown in Fig. 6, is an improved version of the two-layer magnetic coupled resonator. Compared with the configuration in Fig. 2, the structure size remains the same, but a new SRR element on the same substrate is added below the excited loop on the bottom, which has the same sizes but with opposite spit direction with respect to the SRR on the top.

The simulated reflection coefficients of the three-layer resonator and the two-layer resonator are compared in Fig. 7. When the anti-symmetric and opposite-split SRR element is added, this three-layer magnetic coupled resonator operates at 0.39 GHz with 1.1422 MHz impedance bandwidth (from 0.3894073 GHz to 0.3905495 GHz), 0.29% fractional bandwidth and Q-factor of 345. By comparison with the

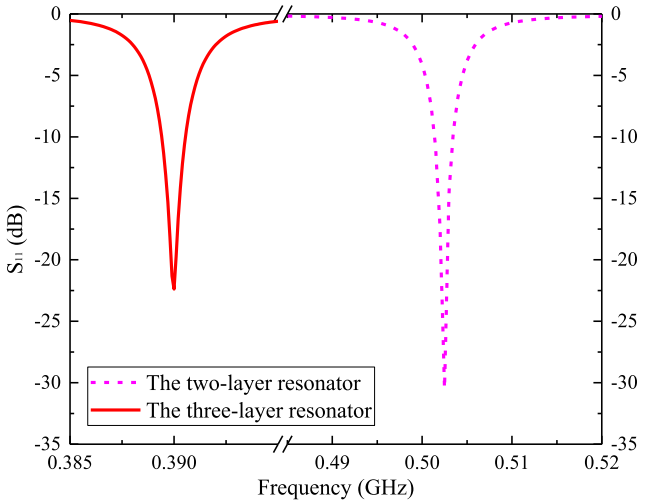

FIGURE 7. Simulated reflection coefficients of the two-layer resonator and three-layer resonator.

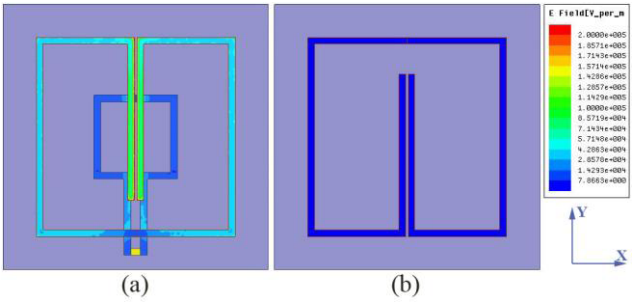

FIGURE 8. Electric field distributions of the three-layer resonator at 0.39 GHz. (a) Top view, (b) bottom view.

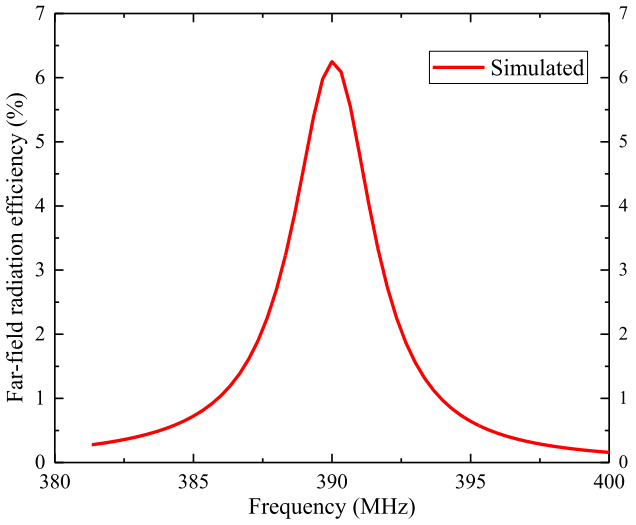

FIGURE 9. Far-field radiation efficiency of the three-layer resonator.

two-layer resonator, this improved three-layer design has a 22.4% lower resonant frequency and achieves a much higher Q-factor under the same physical size. Therefore, this three-layer resonator achieves smaller electrically size than the

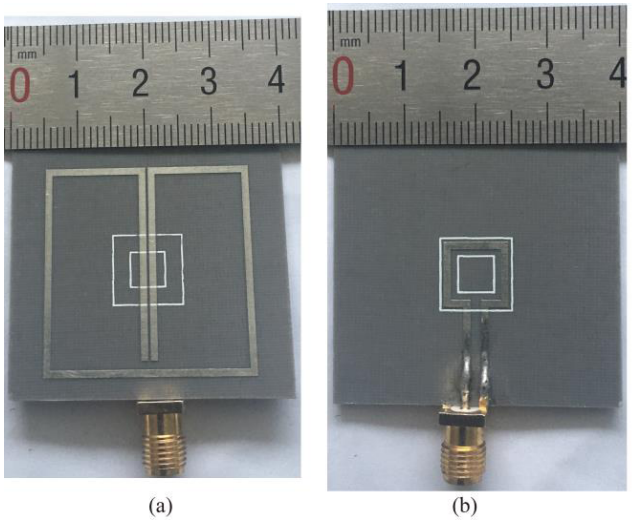

FIGURE 10. Fabricated prototype of the two-layer resonator. (a) Top view, (b) bottom view.

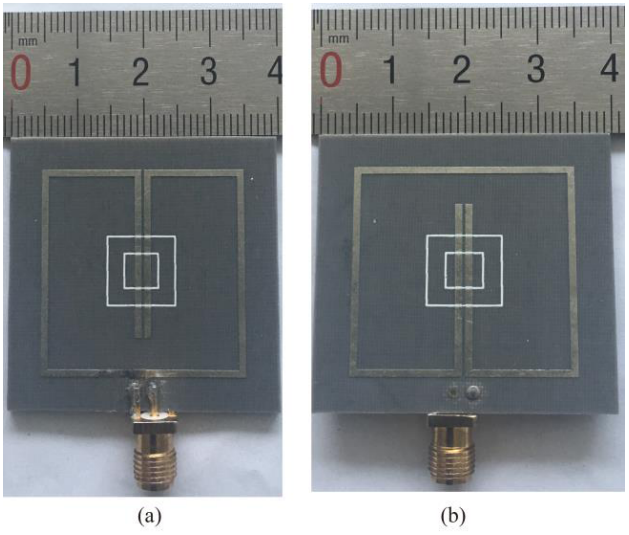

FIGURE 11. Fabricated prototype of the three-layer resonator. (a) Top view, (b) bottom view.

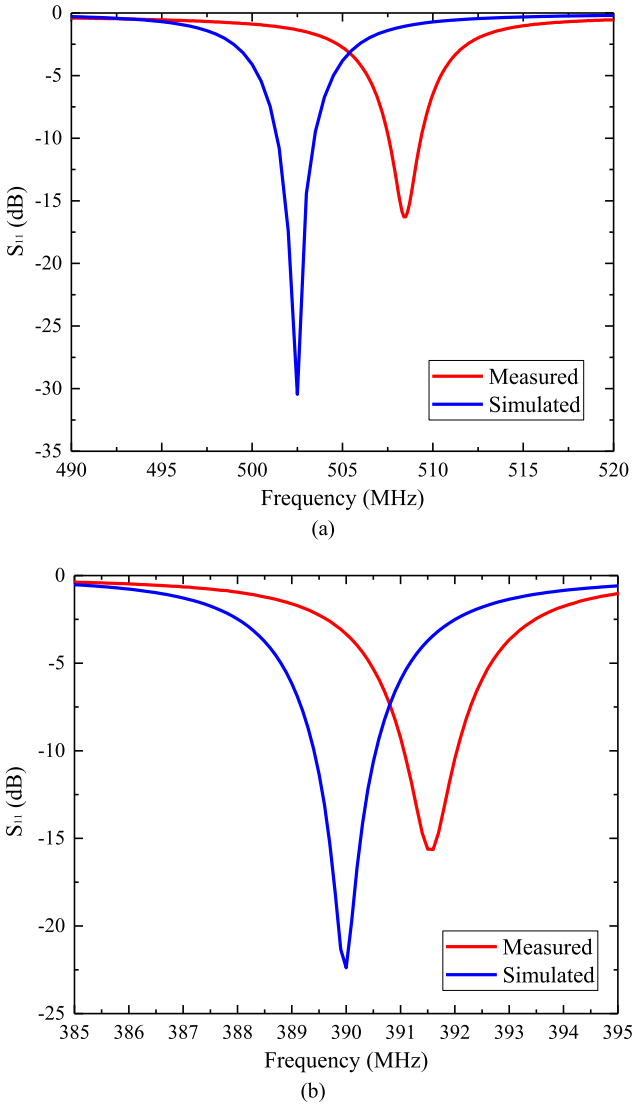

FIGURE 12. Simulated and measured reflection coefficients for unloaded cases (a SUT with a dielectric constant value of 1) with (a) the two-layer resonator, (b) the three-layer resonator.

previous two-layer design, i.e., its electrically size is as small as $0.052\lambda_0 \times 0.052\lambda_0$.

Likewise, the electric field distributions of the top, middle and bottom layers at resonant frequency, i.e., 0.39 GHz are studied. As shown in Fig. 8, owing to the introducing of the anti-symmetry SRR element, the magnetic coupling paths of the intermediate loop are increased. The coupled magnetic fields are distributed into the SRRs on the top and the bottom layers, respectively. The electric field intensity on both SRRs is weaker than these in the two-layer resonator. Since the split of the SRR on the bottom is towards the negative Y-axis and the direction of surface current is opposite to that in the middle magnetic coupled loop, so the intensity of magnetic coupling is much weaker than that in the top layer. As seen in Fig. 8, the maximum electric field distribution of the three-layer resonator is still located on the top of two parallel stubs, and thus the SUT position remains unchanged.

In order to show that the newly introduced anti-symmetric coupled SRR can further effectively suppress the far-field radiation, the radiation efficiency of the three-layer resonator is plotted in Fig. 9. The radiation efficiency at resonance is about 6.3%, which is approximately one half of that in the two-layer resonator. The reason on this reduction can be explained by the efficiency expression (5). When the displacement current of the SRR on the bottom is opposite to that of the SRR on the top layer, the part of $\left(\sum I_n\right)^2$ is then smaller and the denominator of the expression becomes larger, thereby leading to smaller radiation efficiency. Therefore, the proposed three-layer resonator not only has more compact electrically size but also is more stable, robust and immune to the noise from the environment.

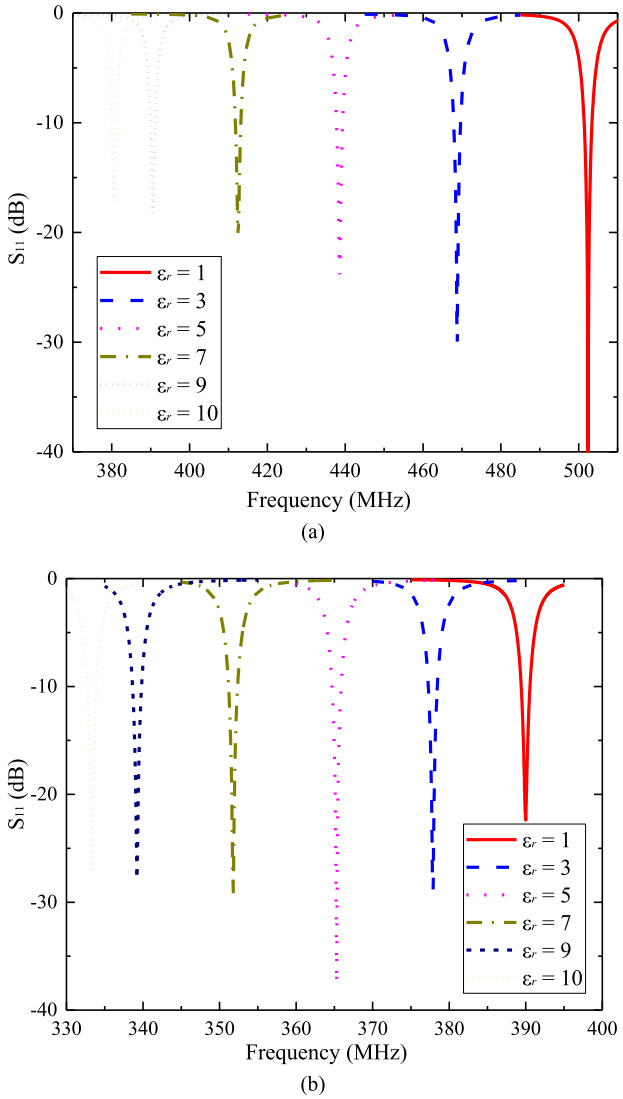

FIGURE 13. Simulated reflection coefficients under various dielectric constant of SUTs. (a) Two-layer resonator, (b) three-layer resonator.

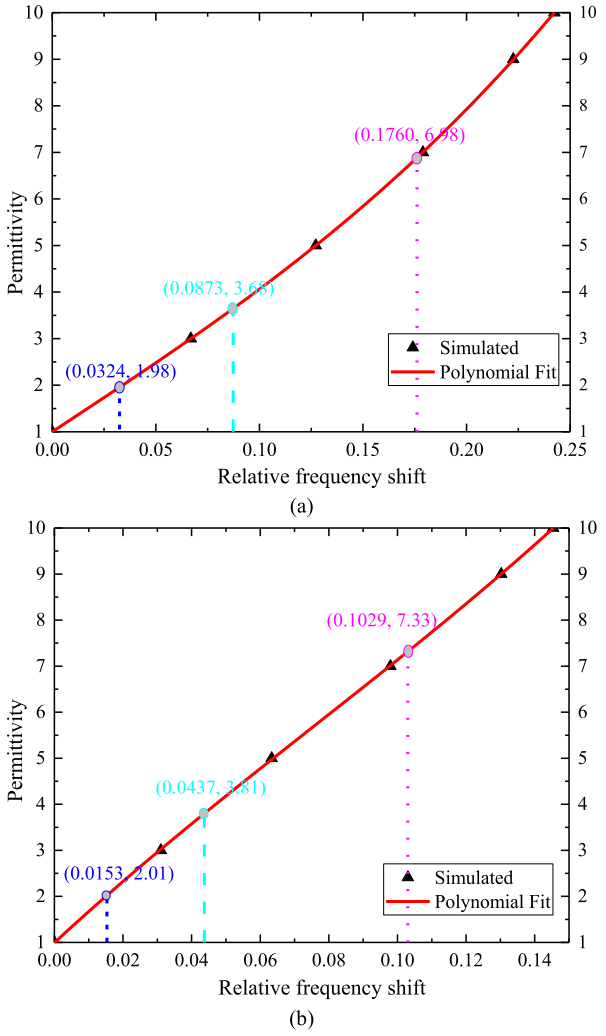

FIGURE 14. Fitting curves. (a) Two-layer resonator, (b) three-layer resonator.

V. EXPERIMENTAL MEASUREMENT

In order to verify the performance of the resonators for permittivity measurement, the experimental prototypes of those two resonators have been fabricated, as shown in Fig. 10 and Fig. 11. The two-layer resonator is directly fed by 50 Ohm SMA connector, while the three-layer resonator is connected to the magnetic coupled loop on the middle layer through the metal via and fed by 50 Ohm SMA. The performances of those two resonators are measured by using Agilent E8363B vector network analyzer. Since the far-field radiations of those two resonators are greatly suppressed, the measurement process can be performed in the open environment.

In the measurement, when the relative permittivity of the SUT is 1 (i.e., there is nothing on the resonators), both the simulated and measured reflection coefficients for the two-layer resonator and the three-layer resonator are shown in Figs. 12(a) and (b), respectively. It can be seen that, the measured results reasonably agree with the simulated results, the slight frequency deviation (i.e., several MHz) between the simulated and measured results mainly come from the dielectric constant uncertainty of the dielectric substrate, the difference of setups such as the feeding definitions and the irresistible factor in the manufacturing process. The slight frequency shift between the simulated and measured results does not affect the measurement of dielectric constant.

To determine the dielectric constant of unknown SUTs, the fitting method with shifting resonant frequency is used to retrieve the relative permittivity. The key of this method is to obtain the formula between the relative shifting resonant frequency and the relative permittivity of the SUTs. Therefore, a formula for the relationship should be got by polynomial fitting from the simulated results.

The reflection coefficients under various dielectric constants of SUTs are depicted in Figs. 13(a) and (b) for the two kinds of resonators, respectively. It can be seen that the two novel resonators have stable and balanced performance

TABLE 2. The retrieved results with the two-layer magnetic coupled resonator.

	Resonant frequency (MHz)	Relative shifting frequency $\Delta f = \lvert f_{ref} - f \rvert / f_{ref}$	Retrieved permittivity	Fitted Polynomial
Simulated results	502.4	0	1	$F_x = B_3 x^3 + B_2 x^2 + B_1 x + B$
	468.8	0.066878981	3	
	438.5	0.12718949	5	
	412.5	0.178941083	7	$B = 1.00039$
	390.6	0.222531847	9	$B_1 = 29.2964$
	380.6	0.242436306	10	$B_2 = -0.24048$
Measured results	508.4 (Air)	0	1	$B_3 = 134.50929$
	491.9 (Teflon)	0.03245476	1.98	$R^2 = 0.99999$
	464 (PMMA)	0.087332809	3.68	
	418.9 (Alumina)	0.176042486	6.98	

TABLE 3. The retrieved results with the three-layer magnetic coupled resonator.

	Resonant frequency (MHz)	Relative shifting frequency $\Delta f = \lvert f_{ref} - f \rvert / f_{ref}$	Retrieved permittivity	Fitted Polynomial
Simulated results	390	0	1	$F_x = B_3 x^3 + B_2 x^2 + B_1 x + B$
	377.9	0.031025641	3	
	365.3	0.063333333	5	
	351.8	0.097948718	7	$B = 0.99393$
	339.2	0.13025641	9	$B_1 = 68.98289$
	333.3	0.145384615	10	$B_2 = -135.15923$
Measured results	391.6 (Air)	0	1	$B_3 = 595.54592$
	385.6 (Teflon)	0.015321757	2.01	$R^2 = 0.99994$
	374.5 (PMMA)	0.043667007	3.81	
	351.3 (Alumina)	0.102911134	7.33	

under different SUTs with various dielectric constants. The resonant frequencies of the two-layer resonator change from 502.4 MHz to 380.6 MHz (i.e., 24.24% relative frequency shift), while the resonant frequencies of the three-layer resonator change from 390 MHz to 333.3 MHz (i.e., 14.54% relative frequency shift). However, if one just utilizes the resonant frequency shift in the simulation to establish the fitting polynomial by which the dielectric constant of the unknown SUTs is calculated with the measured S_{11}, it may lead to faulty results. The inaccurate results are mainly attributed to the difference between the simulated resonant frequencies and the measured ones. Another solution to the problems is that the relationship between measured resonant frequencies and the dielectric constants of known samples is used to obtain the formula. However, this method has great limitations and difficulties, because not only are there many known samples (i.e., accuracy dielectric constants), but also it requires recalibration whenever the measured environment changes.

To circumvent the above difficulties, the relationship between the simulated relative shifting resonant frequency (with respect to the reference frequency of the unloaded cases) and the corresponding dielectric constant used in the simulation is employed to establish the final fitting polynomial. The resonant frequencies with the unknown SUTs are firstly measured and then the relative shifting resonant frequency is calculated to deduce the unknown dielectric constant according to the previously obtained fitting polynomial formula. The relative shifting frequency Δf can be calculated as

$$\Delta f = \frac{|f_{ref} - f|}{f_{ref}}, \tag{6}$$

where f_{ref} is the reference resonant frequency, which is usually the resonant frequency of the unloaded case, and f is the resonant frequency with the unknown SUT on the resonator. The simulated and measured resonant frequencies and the corresponding results of the two kinds of resonators are listed in Table 2 and Table 3, respectively. The cubic polynomials are used to fit the simulated data of the relative shifting frequency versus the corresponding dielectric constant. The fitting curves are depicted in Figs. 14(a) and (b) for the two kinds of resonators, respectively. In the fitting process, the resonant frequencies with dielectric constant of 1 (i.e., the

unloaded cases) for both resonators are used as the reference frequencies. As shown in Table 2 and Table 3, the fitting degrees, i.e., R^2, are almost 100%.

In the measurement, the unloaded cases (i.e., with air) are measured as the references. The resonant frequencies with the different unknown SUTs such as Teflon, PMMA, alumina ceramic samples are measured such that the relative frequency shifts can be calculated by using (6). Finally, the unknown dielectric constants of different SUTs can be obtained with the fitting polynomials above. The measured resonant frequencies of Teflon, PMMA and alumina ceramic samples with the two-layer resonator are 491 MHz, 464 MHz, and 418.9 MHz, respectively, whereas the ones with three-layer resonator are 385.6 MHz, 374.5 MHz, and 351.3 MHz, respectively. The relative shifting frequencies in the loaded cases are listed in two tables. As can be seen from Figs. 14(a) and (b), the final measured dielectric constants of three different SUTs with the two-layer resonator are 1.98, 3.68 and 6.98, while the ones with the three-layer resonator are 2.01, 3.81 and 7.33, respectively. As is well known, the relative permittivity of Teflon is about 2. It can be seen that the dielectric constants measured by both resonators are nearly equal to 2, which validate the accuracy and stability of the proposed methods. The measured errors are mainly due to the unavoidable influence from the surrounding environment, the unavoidable position variation where the SUTs are placed, and so on. Even so, the measured errors in two methods are quite small and can be considered as acceptable and under well control.

VI. CONCLUSION

In this work, two kinds of electrically small resonators (i.e., two- and three-layer magnetic coupled SRRs) have been proposed by virtue of novel SRRs to measure the permittivity of unknown SUTs with the resonant methods. Compared with the two-layer resonator, the proposed three-layer resonator has higher sensitivity, better stability and stronger anti-jamming ability from the external interference. The ultralow far-field radiations made the proposed microwave sensors independent from specific experimental environment. In the post-processing algorithm, the relative shifting frequencies were used to fit the formula which relates the dielectric constants to the resonant frequencies, which makes the measurement system more robust against with the noise and some unavoidable errors in the measurement. Although the contact measurement is herein employed to validate the methods, but it also can be readily to be extended to the non-contact measurement in the near field. Under the methodology of multilayer magnetic coupling SRRs, those proposed novel resonators can be readily applied to higher microwave and millimeter wave frequencies. With merits of electrically small size, ultralow far-field radiation, good stability, robustness against to noise and frequency scalability, these proposed resonators and measurement methods can be widely applied to many industry practical applications.

REFERENCES

[1] U. Kaatze and Y. Feldman, "Broadband dielectric spectrometry of liquids and biosystems," *Meas. Sci. Technol.*, vol. 17, no. 2, pp. R17–R35, Feb. 2006.

[2] S. O. Nelson and S. Trabelsi, "Dielectric spectroscopy measurements on fruit, meat, and grain," *Trans. Amer. Soc. Agricult. Biol. Eng.*, vol. 51, no. 5, pp. 1829–1834, Sep. 2008.

[3] Y. Hong, H.-J. Lee, S.-G. Kim, B.-H. Kim, G.-H. Yun, and J.-G. Yook, "A label-free biosensing platform using a PLL circuit and biotin-streptavidin binding system," *IEEE Trans. Biomed. Circuit Syst.*, vol. 9, no. 3, pp. 345–352, Jun. 2015.

[4] V. Sekar, W. J. Torke, S. Palermo, and K. Entesari, "A self-sustained microwave system for dielectric-constant measurement of lossy organic liquids," *IEEE Trans. Microw. Theory Techn.*, vol. 60, no. 5, pp. 1444–1455, May 2012.

[5] N. Suwan, "Investigation of RF direct detection architecture circuits for metamaterial sensor applications," M.S. thesis, Dept. Elect. Comput. Eng., Univ. Waterloo, Waterloo, ON, Canada, 2011.

[6] H. Suzuki, T. Hotchi, and T. Nojima, "A new measurement system for the perpendicular complex permittivity to DUT sheet by stripline simulation," *IEEE Trans. Instrum. Meas.*, vol. 61, no. 9, pp. 2476–2482, Sep. 2012.

[7] M. N. M. Kehn, L. Shafai, F. Safari, and S. Noghanian, "Permittivity measurement of disk and annular dielectric samples using coaxial transmission line fixtures. Part II: Experimentation and accuracy analyses," *Can. J. Elect. Comput. Eng.*, vol. 34, nos. 1–2, pp. 31–41, 2009.

[8] A. M. Hassan, J. Obrzut, and E. J. Garboczi, "A *Q*-band free-space characterization of carbon nanotube composites," *IEEE Trans. Microw. Theory Techn.*, vol. 64, no. 11, pp. 3807–3819, Nov. 2016.

[9] A. Rashidian, L. Shafai, D. Klymyshyn, and C. Shafai, "A fast and efficient free-space dielectric measurement technique at mm-wave frequencies," *IEEE Antennas Wireless Propag. Lett.*, vol. 16, pp. 2630–2633, 2017.

[10] Z. Akhter and M. J. Akhtar, "Free-space time domain position insensitive technique for simultaneous measurement of complex permittivity and thickness of lossy dielectric samples," *IEEE Trans. Instrum. Meas.*, vol. 65, no. 10, pp. 2394–2405, Oct. 2016.

[11] M. Ndoye, H. El Matbouly, Y. N. Sama, D. Deslandes, and F. Domingue, "Sensitivity evaluation of dielectric perturbed substrate integrated resonators for hydrogen detection," *Sens. Actuators A, Phys.*, vol. 251, pp. 198–206, Nov. 2016.

[12] S. P. Chakyar, S. K. Simon, C. Bindu, J. Andrews, and V. P. Joseph, "Complex permittivity measurement using metamaterial split ring resonators," *J. Appl. Phys.*, vol. 121, no. 5, p. 054101, Jan. 2017.

[13] M. S. Boybay and O. M. Ramahi, "Material characterization using complementary split-ring resonators," *IEEE Trans. Instrum. Meas.*, vol. 61, no. 11, pp. 3039–3046, Nov. 2012.

[14] C.-S. Lee and C.-L. Yang, "Thickness and permittivity measurement in multi-layered dielectric structures using complementary split-ring resonators," *IEEE Sensors J.*, vol. 14, no. 3, pp. 695–700, Mar. 2014.

[15] R. A. Alahnomi, Z. Zakaria, E. Ruslan, S. R. Ab Rashid, and A. A. M. Bahar, "High-Q sensor based on symmetrical split ring resonator with spurlines for solids material detection," *IEEE Sensors J.*, vol. 17, no. 9, pp. 2766–2775, May 2017.

[16] Y. Li, N. Bowler, and D. B. Johnson, "A resonant microwave patch sensor for detection of layer thickness or permittivity variations in multilayered dielectric structures," *IEEE Sensors J.*, vol. 11, no. 1, pp. 5–15, Jan. 2011.

[17] J. Han and W. Geyi, "A new method for measuring the properties of dielectric materials," *IEEE Antennas Wireless Propag. Lett.*, vol. 12, pp. 425–428, 2013.

[18] K. Saeed, R. D. Pollard, and I. C. Hunter, "Substrate integrated waveguide cavity resonators for complex permittivity characterization of materials," *IEEE Trans. Microw. Theory Techn.*, vol. 56, no. 10, pp. 2340–2347, Oct. 2008.

[19] E. Fratticcioli, M. Dionigi, and R. Sorrentino, "A simple and low-cost measurement system for the complex permittivity characterization of materials," *IEEE Trans. Instrum. Meas.*, vol. 53, no. 4, pp. 1071–1077, Aug. 2004.

[20] F. Shen *et al.*, "Noncontact measurement of complex permittivity based on the principle of mid-range wireless power transfer," *IEEE Trans. Microw. Theory Techn.*, vol. 62, no. 3, pp. 669–678, Mar. 2014.

[21] S. Li, C. Akyel, and R. G. Bosisio, "Precise calculations and measurements on the complex dielectric constant of lossy materials using TM_{010} cavity perturbation techniques," *IEEE Trans. Microw. Theory Techn.*, vol. MTT-29, no. 10, pp. 1041–1048, Oct. 1981.

[22] J. Dong, "Noncontact measurement of complex permittivity of electrically small samples at microwave frequencies," *IEEE Trans. Microw. Theory Techn.*, vol. 64, no. 9, pp. 2883–2893, Sep. 2016.
[23] J. B. Pendry, A. J. Holden, D. J. Robbins, and W. J. Stewart, "Magnetism from conductors and enhanced nonlinear phenomena," *IEEE Trans. Microw. Theory Techn.*, vol. 47, no. 11, pp. 2075–2084, Nov. 1999.
[24] K. T. M. Shafi, A. K. Jha, and M. J. Akhtar, "Improved planar resonant RF sensor for retrieval of permittivity and permeability of materials," *IEEE Sensors J.*, vol. 17, no. 17, pp. 5479–5486, Sep. 2017.
[25] R. Marques, F. Medina, and R. Rafii-El-Idrissi, "Role of bianisotropy in negative permeability and left-handed metamaterials," *Phys. Rev. B, Condens. Matter*, vol. 65, p. 144440, Apr. 2002.
[26] L. Peng, P. Chen, A. Wu, and G. Wang, "Efficient radiation by electrically small antennas made of coupled split-ring resonators," *Sci. Rep.*, vol. 6, p. 33501, Sep. 2016.
[27] K. Xu, F. Liu, L. Peng, W.-S. Zhao, L. Ran, and G. Wang, "Multimode and wideband printed loop antenna based on degraded split-ring resonators," *IEEE Access*, vol. 5, pp. 15561–15570, 2017.

KUIWEN XU received the B.E. degree from Hangzhou Dianzi University, Hangzhou, China, in 2009, and the Ph.D. degree from Zhejiang University, Hangzhou, in 2014. He was a Visiting Ph.D. Student with the National University of Singapore, Singapore, from 2012 to 2013.

From 2014 to 2015, he was with Huawei Technologies Co. Ltd. He is currently an Associate Professor with Hangzhou Dianzi University. He is also with the State Key Laboratory of Millimeter waves, Southeast University, Nanjing, China. His research interests include antenna design, microwave measurement, and electromagnetic inverse problems.

YANG LIU received the B.S. degree in electronic information engineering from the Zhixing College of Hubei University, Wuhan, China. He is currently pursuing the M.S. degree in electromagnetic field and microwave technology with Hangzhou Dianzi University, Hangzhou, China. His research interests include multiband antenna, printed broadband antenna, electrically small antenna, and microwave sensor.

SHICHANG CHEN (S'09–M'14) received the B.S. and Ph.D. degrees in electronic engineering from the Nanjing University of Science and Technology and the City University of Hong Kong in 2009 and 2013, respectively.

From 2013 to 2014, he was with the City University of Hong Kong as a Post-Doctoral Fellow. He is currently an Associate Professor with Hangzhou Dianzi University. His research interest focuses on high-efficiency power amplifier, integrated circuits, and sensors.

PENG ZHAO (S'12–M'16) received the B.Eng. and M.Phil. degrees from the Electronic Engineering Department, Zhejiang University, China, in 2006 and 2008, respectively, and the Ph.D. degree in electronic engineering from the City University of Hong Kong, Hong Kong, in 2014. He is currently a Faculty Member with the Key Laboratory of RF Circuits and Systems, Ministry of Education, Microelectronics CAD Center, Hangzhou Dianzi University, Hangzhou, China. He is also with the State Key Laboratory of Millimeter waves, Southeast University, Nanjing, China. His research interests include microwave devices and computational electromagnetic.

LIANG PENG received the B.S. and Ph.D. degrees from Zhejiang University, Hangzhou, China, in 2003 and 2008, respectively. He held a post-doctoral position at the Technical University of Denmark from 2009 to 2011. In 2011, he joined Hangzhou Dianzi University, where he became a Research Associate in 2012. His research interests include electromagnetic theory, artificial metamaterials, new concept antennas, optical plasmonics, and topological photonics.

LINXI DONG received the Ph.D. degree in microelectronics and solid electronics from Zhejiang University, Hangzhou, China, in 2004. He is currently a Professor with Hangzhou Dianzi University, where he is involved in the design and fabrication of MEMS sensors, resonators, wireless sensor network, and integrated circuit.

GAOFENG WANG (S'93–M'95–SM'01) received the Ph.D. degree in electrical engineering from the University of Wisconsin–Milwaukee, Milwaukee, WI, USA, in 1993, and the Ph.D. degree in scientific computing from Stanford University, Stanford, CA, USA, in 2001.

He was a Scientist with Tanner Research, Inc., Pasadena, CA, USA, from 1993 to 1996.

He was a Principal Researcher and a Development Engineer with Synopsys, Inc., Mountain View, CA, USA, from 1996 to 2001. In 1999, he served as a Consultant with Bell Laboratories, Murray Hill, NJ, USA. He was the Chief Technology Officer with Intpax, Inc., San Jose, CA, USA, from 2001 to 2003, and Siargo Inc., Santo Clara, CA, USA, from 2004 to 2010. He was a Professor and the Head of the CJ Huang Information Technology Research Institute with Wuhan University, Wuhan, China, from 2004 to 2013. He was the Chief Scientist with Lorentz Solution, Inc., Santa Clara, CA, USA, from 2010 to 2013. He is currently a Distinguished Professor with Hangzhou Dianzi University, Hangzhou. He has authored over 160 journal articles and holds 22 patents. His current research interests include integrated circuit and microelectromechanical system design and simulation, computational electromagnetics, electronic design automation, and wavelet applications in engineering.